NUMERICAL MODEL-BASED DIAGNOSTIC STUDY OF THE INITIAL DEVELOPMENT PHASE OF THE PRESIDENTS' DAY CYCLONE

Louis W. Uccellini[1], Keith F. Brill[2], and Paul J. Kocin[1]

[1]Laboratory for Atmospheres
NASA/Goddard Space Flight Center
Greenbelt, MD 20771
USA

[2]General Sciences Corporation
Laurel, MD 20707
USA

1. INTRODUCTION

The development of primitive equation numerical models during the past 20 years has emphasized predictions of atmospheric phenomena from global-scale circulations to mesoscale weather events. These models can be subdivided into two classes: (1) global models that are designed to simulate the global- to synoptic-scale circulation patterns and (2) regional-scale models that are designed to predict significant weather events associated with synoptic- to mesoscale circulations. A parallel motivation for the development of regional models, as discussed by Keyser and Uccellini (1987), is their potential application to diagnostic studies of mesoscale phenomena that are associated with significant weather events. The regional models have become an effective research tool by providing gridded fields of data possessing a degree of dynamical consistency, spatial coverage, and spatial and temporal resolution exceeding that obtainable from conventional observing systems.

The purpose of this two-part paper is to describe the application of one regional-scale model to a diagnostic study of the "Presidents' Day" snowstorm which produced heavy snow along the East Coast of the United States on 18-19 February 1979 (Bosart, 1981; Bosart and Lin, 1984; Uccellini et al., 1984, 1985). In part I[3], the simulation of the initial development phase of the storm on 18 February 1979, involving secondary

[3]This study is derived from a paper recently published in Monthly Weather Review (Uccellini et al., 1987).

cyclogenesis along the East Coast, is described. A brief review of the Presidents' Day storm is presented in Section 2. A brief description of the model and a model sensitivity study, focusing on the relative contributions of various physical processes during the initial development, is summarized in Section 3. Factors which contribute to the development of a low-level jet streak (LLJ) near the coast are discussed in Section 4, with the effect of the LLJ on the onset of cyclogenesis [marked by a decrease of the sea-level pressure (SLP) along the coast] described in Section 5. The results are summarized in Section 6. The simulation of the rapid development phase of the Presidents' Day storm on 18 February 1979 is described in the second part of this paper.

2. REVIEW OF THE PRESIDENTS' DAY CYCLONE AND DESCRIPTION OF THE LOW-LEVEL JET DURING THE PRECYCLOGENETIC PERIOD

The Presidents' Day cyclone developed along the East Coast of the United States on 18-19 February 1979, producing heavy snow accumulations from North Carolina to southeastern New York. A variety of processes appear to have contributed to various stages of the storm's development, as described in numerous papers listed in Table 1.

Table 1. Diagnostic studies of the Presidents' Day cyclone of 18-19 February 1979.

	Phenomenon/Process	Reference
Precyclogenetic period and initial secondary development (18 February)	1) coastal frontogenesis	Bosart (1981), Uccellini et al. (1987)
	2) diabatic processes	Bosart (1981), Bosart and Lin (1984), Uccellini et al. (1987)
	3) increasingly divergent subtropical jet	Uccellini et al. (1984, 1987)
	4) ageostrophic low-level jet	Uccellini et al. (1984, 1987)
Rapid development phase (19 February)	1) large-scale forcing	Bosart (1981), Bosart and Lin (1984), Uccellini et al. (1984), Atlas (1987)
	2) upstream tropopause folding	Uccellini et al. (1985), Petersen et al. (1985)
	3) heating on the convective scale	Bosart (1981)
	4) other diabatic processes	Bosart and Lin (1984), Uccellini et al. (1985), Atlas (1987)

[4]The time and date format is expressed as follows: 0000 GMT 18 February becomes 00Z/18. All analyses in this paper were derived using Petersen's (1986) objective analysis scheme on a 2° latitude by 2° longitude grid using data sets described by Uccellini et al. (1984).

Since Bosart (1981) and Uccellini et al. (1984) present detailed synoptic analyses of the storm, only a brief description is presented here. At 06Z/18[4], snow, sleet, and rain were occurring in the southern United States with an inverted trough beginning to extend northward from the Gulf of Mexico (Fig. 1a). By 12Z/18, heavy snow developed in the southeastern United States as a separate inverted trough/coastal front began to develop off the Southeast Coast (Fig. 1b). A surface low formed along the coastal front by 18Z/18 (Fig. 1c) and moved northeastward to a position off the South Carolina coast by 00Z/19 (Fig. 1d). The development of the coastal low occurred as a separate surface low formed in the Ohio Valley (Fig. 1d), but did not deepen appreciably. The coastal system continued to intensify, deepening explosively off the Virginia coast after 06Z/19.

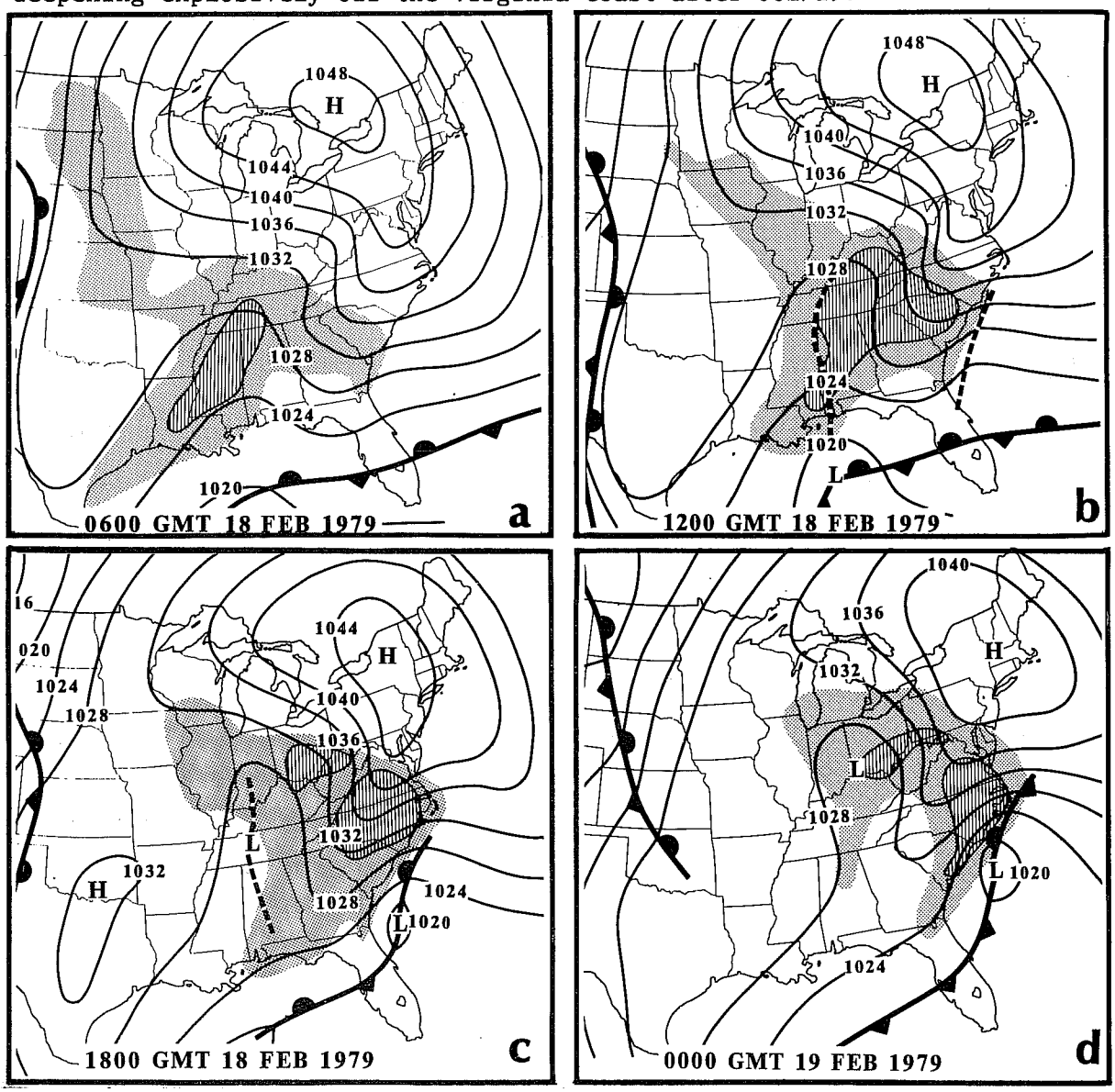

Fig. 1. *Surface analyses (solid lines are isobars, mb) for 0600 GMT 18 February (a), 1200 GMT 18 February (b), 1800 GMT 18 February (c), and 0000 GMT 19 February 1979 (d). Shading represents precipitation with hatched shading representing moderate to heavy precipitation. Dashed lines in (b) and (c) indicate sea-level inverted pressure trough and developing coastal front.*

The period prior to 18Z/18 was marked by significant changes in the upper- and lower-tropospheric wind fields. A subtropical jet (STJ) near 200 mb amplified on 17 and 18 February, with wind speeds increasing 5 m s^{-1} along a significant portion of the jet axis between 00Z/18 and 12Z/18 (Figs. 2a and 2b). Uccellini et al. (1984) diagnose a temporally increasing divergence field along the axis of the STJ upstream of the upper-level ridge crest during this period. As the divergence along the axis of the STJ increased, a LLJ developed in the southeastern United States. Winds near the 850 mb level on the 292 K isentropic surface increased from 5 to 25 m s^{-1} between 00Z/18 and 12Z/18 (Figs. 2c and 2d). The LLJ was directed up sloped isentropic surfaces from about 900 mb (over the ocean) toward the 700 mb level (over the Carolinas) and was an important factor in doubling the magnitude of the moisture transport into the region of heavy snow (Uccellini et al., 1984). The southeasterly LLJ formed at an angle nearly perpendicular to the coastline in a region where the geostrophic wind was south-southwest. As a result, the rapid development of the LLJ was marked by a well-defined 20 m s^{-1} ageostrophic wind component at 12Z/18, in an area where only an ill-defined 5 m s^{-1} ageostrophic wind field had existed 12 h earlier (Uccellini et al., 1984).

The development of the LLJ occurred in the lower branch of an indirect circulation associated with the STJ, as noted by Uccellini et al. (1984). This circulation is depicted in the cross section in Fig. 3 that extends along a line from northern Illinois to a position off the Southeast Coast (see Fig. 2b). The indirect circulation (marked by an "I" in Fig. 3) is displaced to the anticyclonic side of the STJ and is defined by the 3 μb s^{-1} descent of relatively warm air off the coast and 8 μb s^{-1} ascent of relatively colder air beneath the axis of the STJ. The upper- (lower-) tropospheric ageostrophic flow directed toward the anticyclonic (cyclonic) side of the STJ completes the circulation pattern. A significant portion of the troposphere beneath and on the cyclonic side of the STJ axis is marked by a large ageostrophic component directed to the left of the flow. This is consistent with the diagnosed acceleration of parcels along the axis of the STJ and near the ridge crest as described by Uccellini et al. (1984).

The slope of the LLJ from beneath 850 mb to above the 700 mb level within the lower branch of the indirect circulation suggests that a coupling between the upper- and lower-level jets, as discussed by Uccellini and Johnson (1979), may exist for this case. In addition, the occurrence of heavy precipitation beneath the axis of the STJ and the presence of

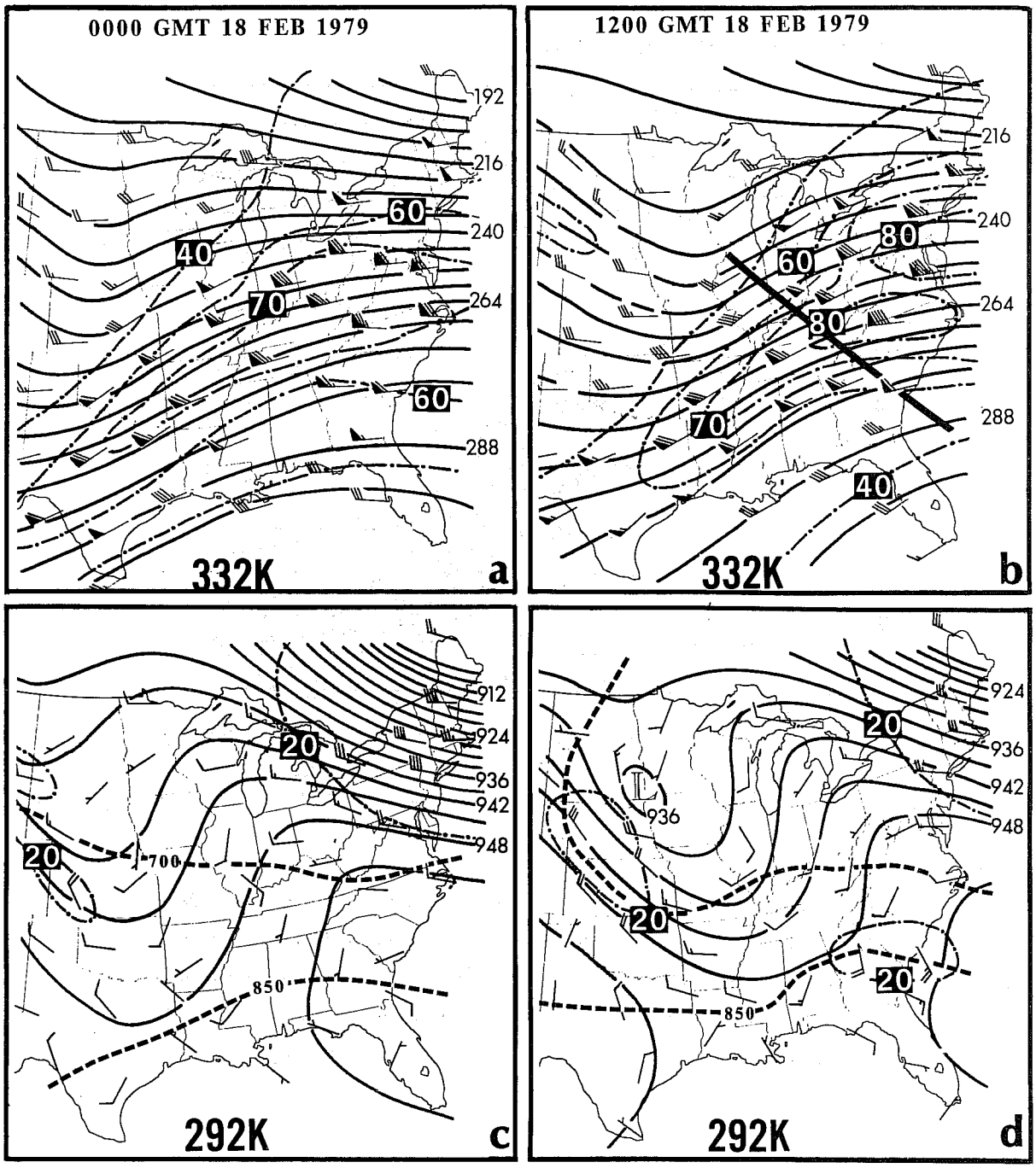

Fig. 2. *Isentropic analyses for 332 K [(a) and (b)] and 292 K [(c) and (d)] at 0000 and 1200 GMT 18 February 1979, respectively. Montgomery streamfunction (ψ_m) (solid, 288 = 3.288 x 10^5 m^2 s^{-2}; 936 = 2.936 x 10^5 m^2 s^{-2}) and isotachs (dot-dashed, m s^{-1}). Wind barbs represent measured velocities (flag = 50 m s^{-1}; barb = 10 m s^{-1}; half-barb = 5 m s^{-1}). Isobars on 292 K surface are dashed (mb). Heavy line in (b) indicates position of cross section in Fig. 3.*

significant sensible heating off the coast for this case (Bosart, 1981; Chou and Atlas, 1982) also suggest that diabatic processes could also be influencing the observed ageostrophic wind fields, which has recently been described for a case involving deep convective storms (Keyser and Johnson, 1984). Furthermore, the location of the LLJ immediately above the

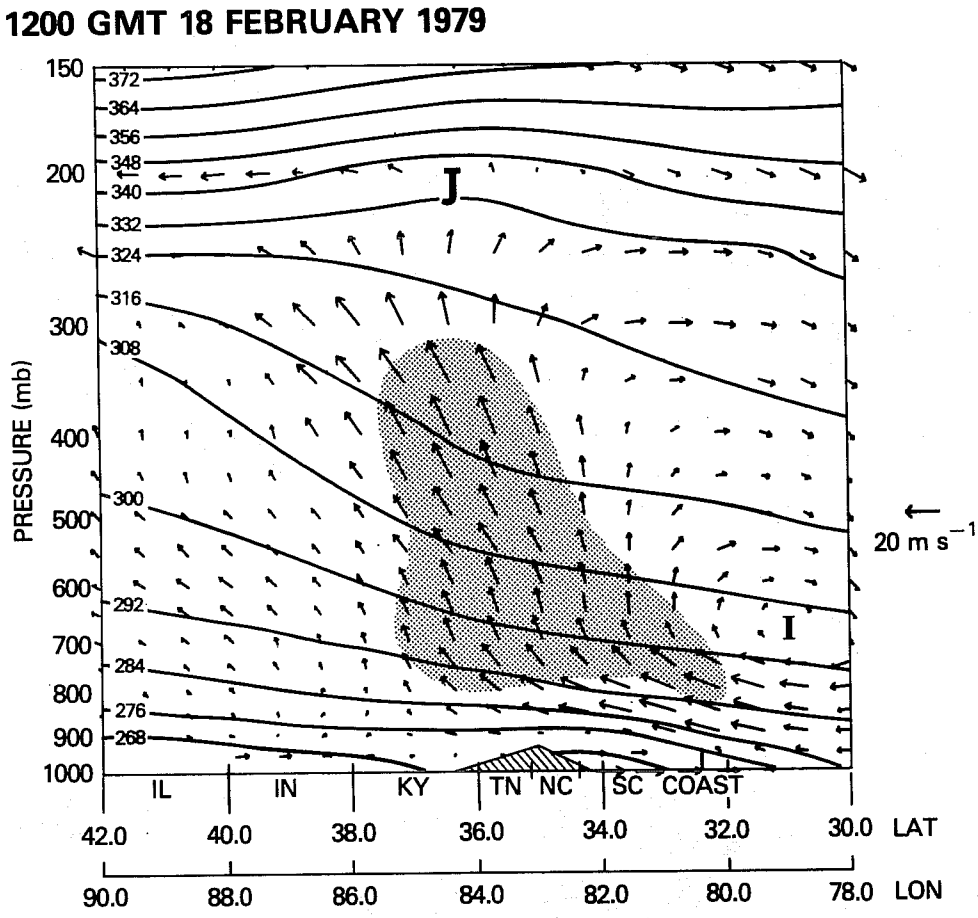

Fig. 3. *Vertical cross section of potential temperature (contour interval 8 K, solid) at 1200 GMT 18 February 1979 and vector representation of ageostrophic indirect (I) circulation derived from the objective analysis scheme (see text for details). Cross section derived along rhumb line illustrated in Fig. 2b. Shading indicates region where ascent is greater than -6 $\mu b\ s^{-1}$. Scale for magnitudes (m s^{-1}) of horizontal component shown on right. "J" indicates position of core of subtropical jet streak (STJ).*

developing coastal front (compare Figs. 1b and 2d) indicates that processes associated with coastal frontogenesis may also be playing a role in the formation of the LLJ. Given that a large number of physical processes may be influencing the rapid evolution of the LLJ between 00Z/18 and 12Z/18 and the subsequent development of the coastal cyclone, a series of numerical simulations is needed to assess the contributions of the adiabatic and diabatic processes in the development of the LLJ and associated SLP falls along the coast.

3. THE NUMERICAL MODEL AND EXPERIMENTAL DESIGN

3.1 Model description

The numerical model used in this study is an updated version of the Mesoscale Analysis and Simulation System (MASS) described by Kaplan et al. (1982a) and modified and transferred to the CYBER 205 at the Goddard Space Flight Center as described by Uccellini et al. (1987). The vertical coordinate, σ, is defined as $(p-p_t)/(p_s-p_t)$ for 24 equally spaced levels, where p is pressure and p_s and p_t are the pressure at the surface and top (100 mb) of the model, respectively. The simulations discussed here were performed on a 60 km grid for a 128 by 96 mesh corresponding to a 40 by 30 subset of the National Meteorological Center's (NMC's) Limited Area Fine Mesh (LFM) grid area covering all of North America and the western Atlantic Ocean to approximately 55° longitude.

Condensation and evaporation of grid-resolvable precipitation are included in the model. Convective precipitation is determined using a modified Kuo (1974) cumulus parameterization scheme with closure parameters specified by Molinari (1982). Diffusion is applied to the prognostic equations for the horizontal wind components, moisture, surface pressure, and temperature using a $K\nabla^4$ operator where K is defined as a diffusion coefficient and is set to 5×10^5 m^4 s^{-1} on the interior grid points of the model domain. The topography used in the model is equivalent to that used in the LFM and is shown in Fig. 4a.

3.2 Initial analyses

For this study, the model simulations are started at 00Z/18, with temperature, moisture, and wind fields generated at 25 mb intervals using a Cressman (1959) analysis and the FGGE gridded data as a first guess. These fields are updated with an isentropic analysis of the operational radiosonde data over a major portion of the contiguous United States and 14 supplemental soundings over the ocean near the East Coast[5]. The procedure

[5]The supplemental soundings were generated by combining ship and buoy reports of surface pressure, temperature, winds, and dewpoint (when available) with mandatory-level data derived from the LFM analyses for the locations indicated in Fig. 4a. These uniformly spaced soundings were used in an attempt to improve the initial conditions over the ocean, especially in the lowest portion of the troposphere. We recognize, however, that mesoscale detail in the temperature, wind, and moisture fields over the ocean cannot be represented in the initial conditions utilizing this approach.

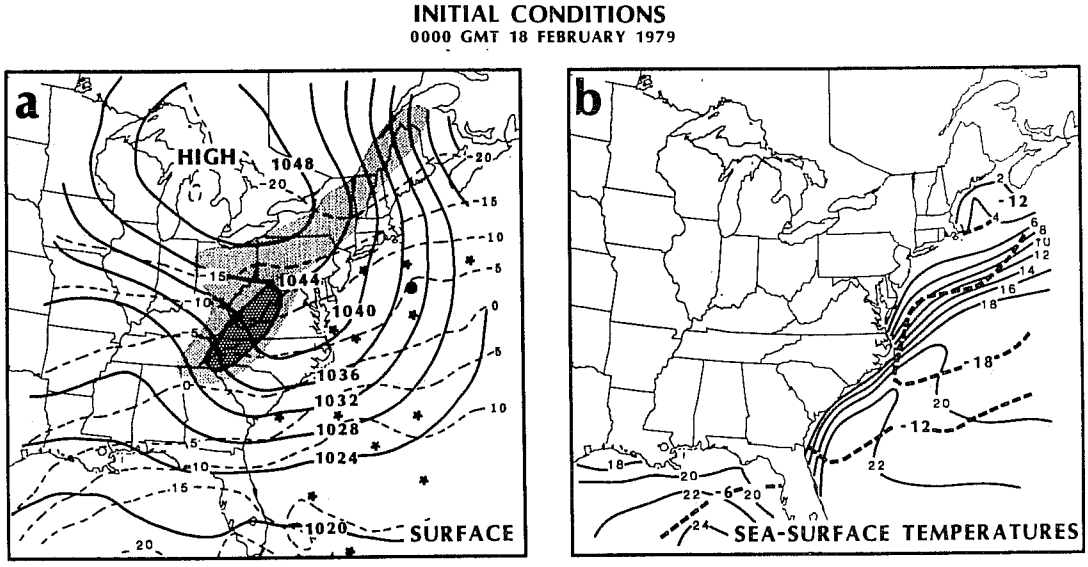

Fig. 4. *Selected initial fields from 0000 GMT 18 February 1979 used in model simulations described in text: (a) sea-level pressure (SLP) (mb, solid) with topography shaded [light shading greater than 250 m above sea level (ASL); dark shading greater than 500 mb ASL] and air temperature for lowest σ model level or approximately 1000 mb (°C, dashed) [the locations of the supplemental soundings are indicated by a (*) and the buoy at 70° W and 39° N by black circle]; (b) climatological sea-surface temperature (SST) (°C, solid) and temperature difference between sea surface and lowest model sigma surface (°C, heavy dashed).*

for inserting the isentropic-based analyzed fields into the model domain is described by Petersen et al. (1985). The model initialization is completed by applying a variational adjustment of temperature under hydrostatic constraint and a variational minimization of the vertically integrated mass divergence and associated surface pressure tendency.

The initial SLP analysis at 00Z/18 (Fig. 4a) is nearly equivalent to that shown in previous studies of the Presidents' Day storm [see, e.g., Fig. 1b in Uccellini (1984)], with a distinct anticyclonic ridge extending southward to the east of the Appalachian Mountains. Extremely cold air associated with this surface high-pressure system is reflected in the temperature analysis on the first model σ level above the ground, which is near 1000 mb (Fig. 4a). In an extensive region off the Middle-Atlantic coast, the air temperature on the lowest model surface is 18°C to 20°C colder than the underlying sea-surface temperature (SST) (Fig. 4b). The existence of very cold air overlying the warm SST is confirmed by Figs. 11 and 12 in Chou and Atlas (1982), where the air temperature of -7°C at a buoy located at 70°W, 39°N at 15Z/17 February is 17°C colder than the SST of 10°C observed at the same location (buoy location is shown in Fig. 4a).

Aloft, the initialized 332 and 292 K fields (not shown), respectively, are nearly identical to those shown in Fig. 2. A divergence maximum of 5.0 x 10^{-5} s^{-1} at the 200 mb level is maintained over Illinois, as was diagnosed for this case [see Fig. 14b in Uccellini et al. (1984)], while the incorporation of the variational adjustment scheme eliminates the "noise" around the perimeter of the domain in which the isentropic analysis was inserted.

3.3 Model experiment

This model experiment consists of four simulations, described in detail by Uccellini et al. (1987).

(1) In the adiabatic simulation (ADB), the latent heat associated with resolvable grid-scale precipitation is not incorporated into the model and the parameterizations for the boundary layer and convective subgrid-scale precipitation are also not operating. Surface stress, however, is applied to the lowest model layer using a procedure described by Haltiner and Williams (1980, pp. 272-274).

(2) In the second simulation (BLYR NO LHT), the boundary layer parameterization is functioning, but the latent heating associated with both the resolvable grid-scale precipitation and convective parameterization is not included. This simulation is designed to isolate the effects of heat and moisture fluxes within the oceanic planetary boundary layer (PBL) without the presence of latent heat release. Therefore, this simulation primarily highlights the role of sensible heating.

(3) In the LHT NO BLYR simulation, both the convective and resolvable grid-scale precipitation routines are operating, but the boundary layer parameterization is not included. This simulation isolates the effect of latent heat release on the coastal system without any additional heat and water vapor supplied from the ocean surface during the course of the numerical forecast.

(4) In the FULL PHYS simulation, all physical parameterizations are included.

The statistical scores derived from the four model simulations listed in Table 2 indicate that the inclusion of heat and moisture fluxes in the oceanic PBL has a significant positive effect on the model simulation of the initial development of the Presidents' Day cyclone by 00Z/19, while latent heating alone yields little improvement over the ADB simulation [for example, compare the statistical scores at 00Z/19 for SLP, temperature (T), and dewpoint temperature (T_d)]. The remarkable improvement in the statistical scores in the BLYR NO LHT versus ADB and LHT NO BLYR simulations for T and T_d near the 1000 mb level points to the importance of surface fluxes in modifying the low-level temperature and moisture structure for this case, where the overlying air mass was significantly colder than the SST [as emphasized by Bosart (1981) and Chou and Atlas (1982)]. However, the detailed diagnostic analyses which follow illustrate that the statistical results taken alone can be misleading. The inclusion of large-scale dynamical processes (associated with the STJ), sensible and latent heat flux in the oceanic PBL, and latent heat release must all be incorporated to improve the model simulation of the LLJ and secondary cyclogenesis for this case.

Table 2. Summary of four model simulations of the Presidents' Day storm of 1979. Statistics computed for 12Z/18 (12-h forecast) and 00Z/19 (24-h forecast) include the root mean square error (RMS), bias (in mb), and S1 score for sea-level pressure (SLP) [along with minimum SLP (mb) along Carolina coast], bias for the first model level (or near 1000 mb) temperature (T) and dewpoint (T_d) in °C, for an area encompassing approximately the eastern half of the United States.

	Statistical Scores							
	SLP:		SLP:		1000 mb T: BIAS		1000 mb T_d: BIAS	
Experiment	Minimum 12Z/18	RMS/BIAS S1 12Z/18	Minimum 00Z/19	RMS/BIAS S1 00Z/19	12Z/18	00Z/19	12Z/18	00Z/19
ADB	1032	2.8/-0.6 40.3	1036	8.2/6.8 53.3	-2.3	-7.4	-7.8	-12.6
BLYR NO LHT	1027	3.4/-2.1 41.7	1024	3.4/2.4 46.3	2.6	-0.6	3.6	1.9
LHT NO BLYR	1032	2.8/-1.1 40.9	1036	7.8/6.3 54.0	-2.6	-7.8	-6.3	-11.4
FULL PHYS	1024	3.8/-2.8 42.8	1017	3.0/0.1 47.5	2.5	-0.7	3.5	1.3

3.4 Summary of the model simulations

In the adiabatic simulation, upper-level divergence is generated along the axis of the STJ as the STJ approaches the crest of an upper-level ridge. As described by Uccellini et al. (1984, 1987), the divergence contributes to the development of an indirect circulation displaced to the anticyclonic side of the jet streak (Fig. 5a). However, the magnitudes of the horizontal and vertical components of this circulation are less than those diagnosed from observations, especially the lower-tropospheric horizontal component. With the inclusion of the diabatic processes associated with sensible and latent heat release (the FULL PHYS simulation), the indirect circulation pattern becomes much better defined (Fig. 5b). The magnitude of the ascending branch is more than doubled from what is generated from the ADB run (5 $\mu b\ s^{-1}$ in ADB; 12 $\mu b\ s^{-1}$ in FULL PHYS), which is consistent with other model sensitivity studies which demonstrate a similar impact of latent heat release on jet-streak-induced transverse circulations (i.e., Cahir, 1971) within the lower branch of the indirect circulation.

The vertical cross sections constructed for FULL PHYS at 12Z/18 (Fig. 5b) also reveal the distinct frontogenesis along the coastline (reflected by the increase of the horizontal gradient of potential temperature immediately along the coast in the plane of the cross section) which does not appear in the ADB cross sections. Associated with the coastal frontogenesis is a shallow direct circulation (indicated by a "D" in Fig. 5c) which is marked by a separate ascent maximum exceeding $-10\ \mu b\ s^{-1}$ in the warmer air to the east of the coastal front and descent (especially near 900 mb) in the colder air to the west. The upper horizontal branch of the direct circulation associated with the coastal front appears to merge with the lower horizontal branch of the indirect circulation associated with the STJ near the 850 mb level.

The greater magnitude of the lower branch of the indirect circulation in FULL PHYS over ADB is apparent in the 292 K wind field in the southeastern United States (Fig. 6). To begin, there is no indication of an organized LLJ on the 292 K surface in the adiabatic simulation (Fig. 6a). In FULL PHYS, wind speeds increase from 10 to greater than 20 $m\ s^{-1}$ over South Carolina between 06Z/18 and 12Z/18 with the wind directed from the southeast over the Carolina coast (not shown). By 18Z/18, the 292 K surface descends to a pressure near the 850 mb level along the coast and wind speeds continue to increase on the isentropic surface, exceeding 30 $m\ s^{-1}$ over South and North Carolina (Fig. 6b).

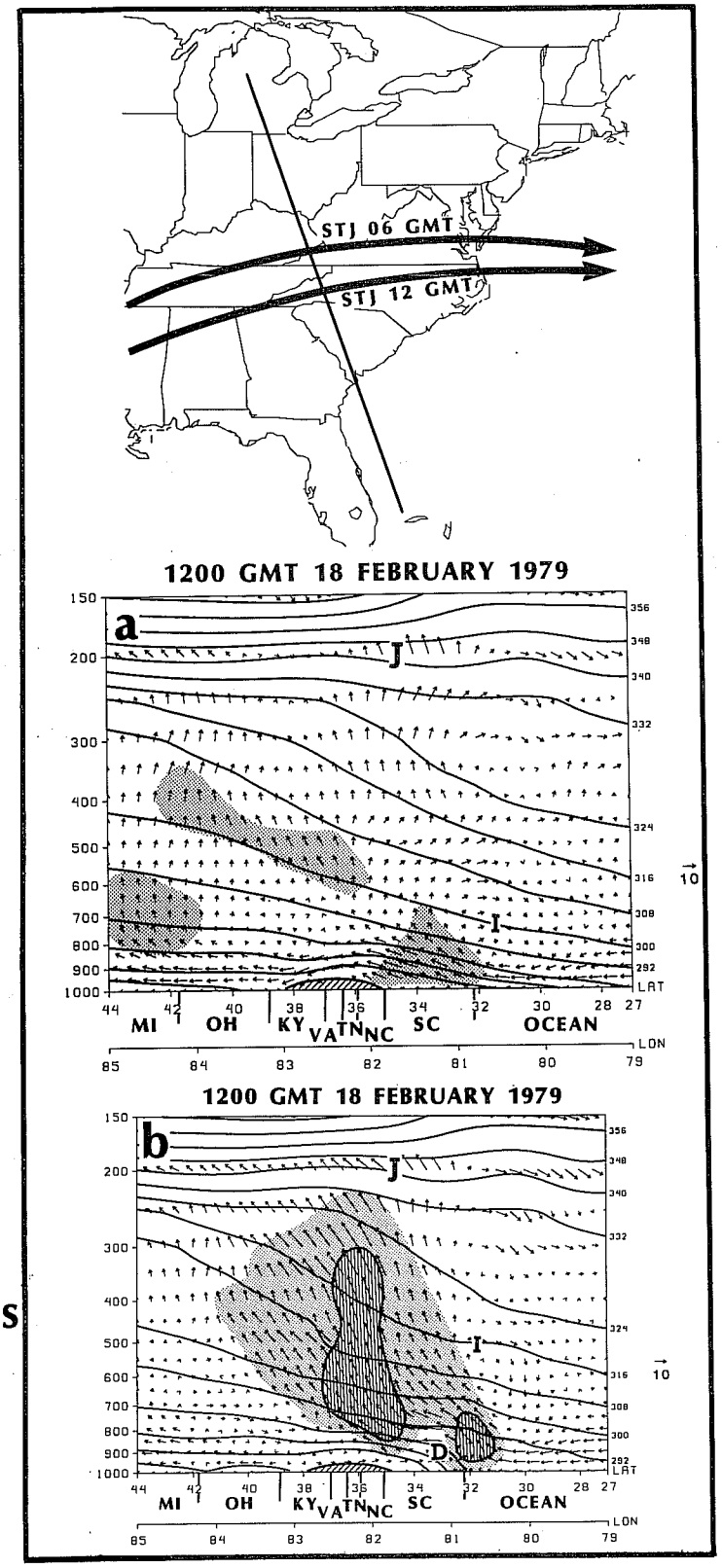

Fig. 5. *Vertical cross sections of transverse ageostrophic component, vertical velocity, and potential temperature derived at 1200 GMT 18 February 1979 and interpolated to vertical plane located along a rhumb line intersecting the subtropical jet streak (STJ) (map inset): (a) from adiabatic simulation (ADB); (b) from full physics simulation (FULL PHYS). See caption for Fig. 3 for details, except that shading indicates the region where ascent is greater than -4 $\mu b\ s^{-1}$ and hatched shading represents ascent greater than -8 $\mu b\ s^{-1}$.*

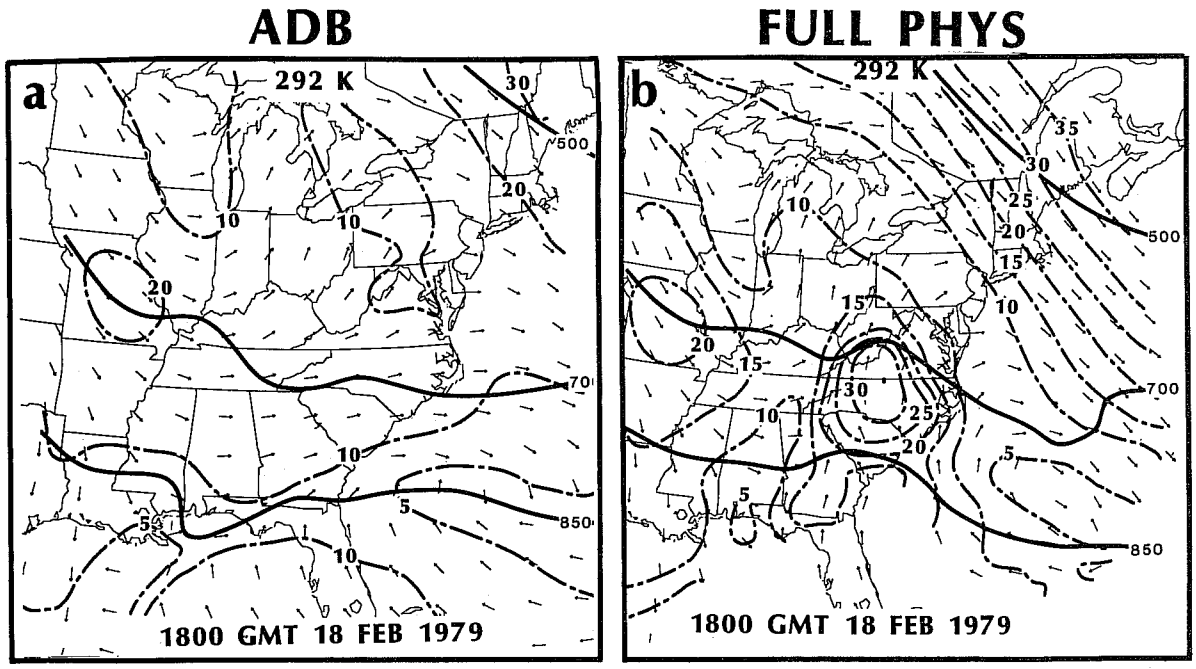

Fig. 6. *The 292 K analyses of wind direction (arrows), isotach (dot-dashed), and selected isobars (mb, solid) at 1800 GMT 18 February 1979 from (a) the adiabatic simulation (ADB) and (b) the full physics simulation (FULL PHYS).*

At sea level, the development of an inverted trough remains weak in both ADB (Fig. 7a) and LHT NO BLYR (Fig. 7b). With the inclusion of heat and moisture fluxes in the boundary layer (BLYR NO LHT), a better-defined inverted trough is simulated (Fig. 7c). Nevertheless, the combination of boundary layer physics and latent heat release (FULL PHYS) is needed for the most accurate simulation of the inverted trough/coastal front (Fig. 7d). As indicated in Table 3, the inclusion of either diabatic processes associated with an ocean-influenced PBL or latent heat of condensation leads to an increase in the lower-tropospheric wind between 06Z/18 and 12Z/18 and a decrease in the minimum SLP. However, the separate contributions are not sufficient by themselves to yield a LLJ or surface low along the coast that satisfactorily matches the observations. Although the separate inclusion of sensible heating yields a coastal front and modest inverted trough, it is not sufficient to ensure the continued development of the secondary cyclone after 18Z/18. Yet, without the contributions of the moisture and heat flux in the ocean boundary layer to the developing precipitation region, the latent heat of condensation is also not sufficient to amplify the lower-tropospheric wind fields to the observed levels, nor to produce the development of an inverted trough and surface low along the coast. Table 3 shows that the difference in the

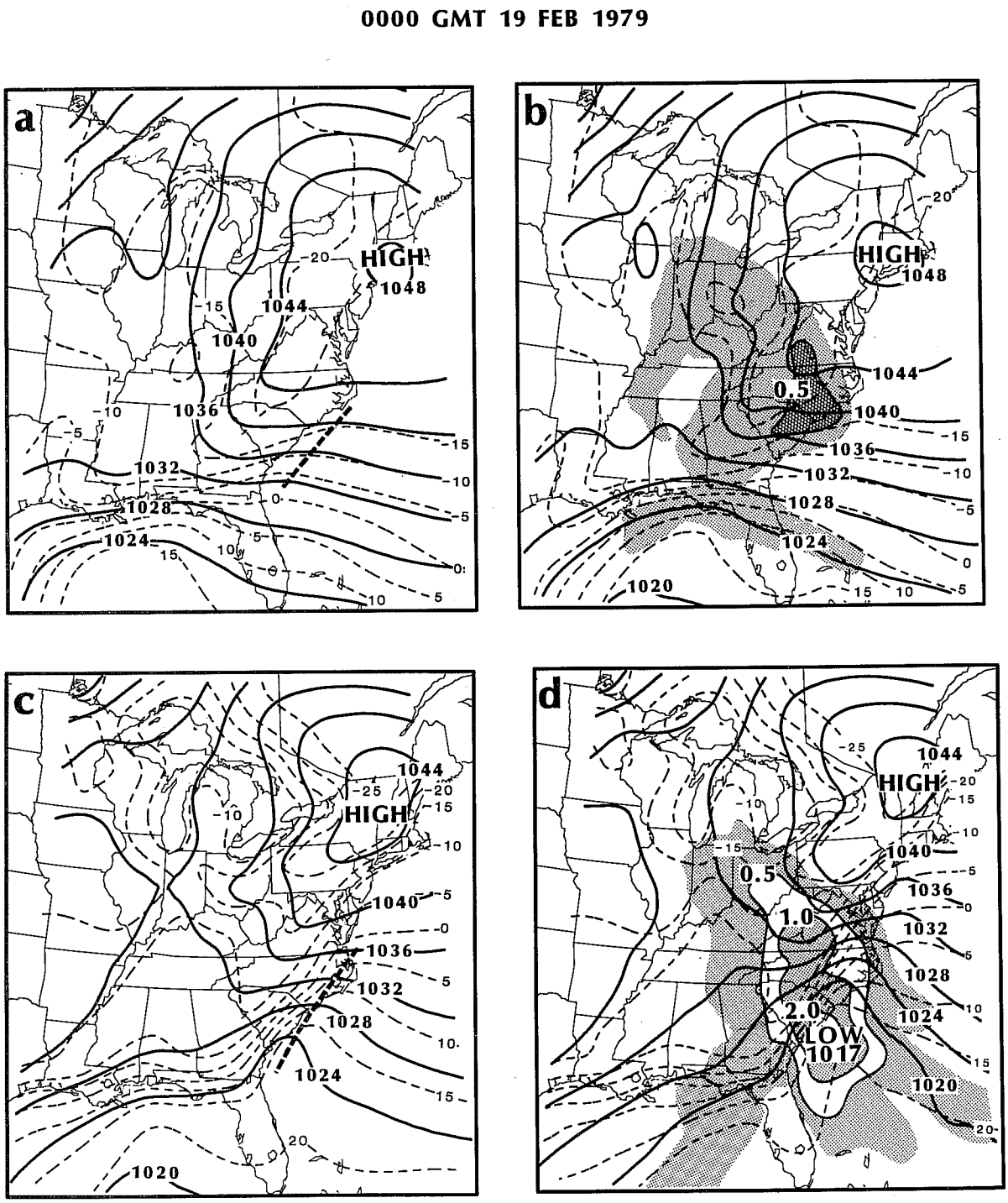

Fig. 7. *The 24-h forecast (valid at 0000 GMT 19 February 1979) of sea-level pressure (SLP) (solid, mb) and isotherms (dashed, °C) for the lowest model level (near 1000 mb) for (a) the adiabatic simulation (ADB), (b) the latent heat no boundary layer simulation (LHT NO BLYR), (c) the boundary layer no latent heat simulation (BLYR NO LHT), and (d) the full physics simulation (FULL PHYS). Thick dashed line represents inverted SLP trough. Shaded intervals in (b) and (d) represent measurable 6-h precipitation amounts (cm).*

maximum 850 mb wind speed between ADB and FULL PHYS at 12Z/18 (13 m s^{-1}) cannot be accounted for by simply adding the difference between BLYR NO LHT and ADB (6 m s^{-1}) and the difference between LHT NO BLYR and ADB (3 m s^{-1}). Likewise, the difference in SLP at 00Z/19 between the ADB and FULL PHYS (19 mb) cannot be accounted for by adding the difference between BLYR NO LHT and ADB (12 mb) and the difference between LHT NO BLYR and ADB (0 mb). These results demonstrate that the LLJ, secondary cyclogenesis, and coastal front can only be properly simulated for this case when these diabatic processes interact synergistically with the dynamical processes associated with the upper-level jet.

In the following sections, trajectory computations and model diagnostics are presented to show (1) how the jet-streak-related dynamical processes and diabatic processes contribute to the development of the LLJ and (2) how the parcel accelerations associated with the LLJ formation act to focus the surface pressure falls along the coast, a process which constitutes the incipient development of the cyclone.

Table 3. Comparison of 1) maximum 850 mb wind speed (m s^{-1}) for LLJ feature in southeastern United States for 06Z/18 and 12Z/18 and 2) minimum sea-level pressure (SLP; mb) for location just off South Carolina coast for the times indicated, for the four model simulations listed in Table 2.

Experiment	Maximum 850 mb Wind		Minimum SLP				
	06Z/18	12Z/18	00Z/18	06Z/18	12Z/18	18Z/18	00Z/19
ADB	5	18	1032	1032	1032	1035	1036
BLYR NO LHT	5	24	1032	1030	1027	1027	1024
LHT NO BLYR	6	21	1032	1030	1032	1036	1036
FULL PHYS	6	31	1032	1028	1024	1022	1017

4. THE DEVELOPMENT OF THE LOW-LEVEL JET

As described in Section 3, the FULL PHYS simulation produces a LLJ that extends from below 850 mb near the coastline to above 700 mb over the Appalachian Mountains. It appears that the LLJ develops in the region where the lower branch of an indirect circulation associated with the STJ and the upper branch of the direct circulation associated with coastal frontogenesis and damming merge near the 850 mb level.

The development of the LLJ in the FULL PHYS simulation is portrayed utilizing hourly sequences of the 850 mb total ($\underset{\sim}{U}$) and ageostrophic ($\underset{\sim}{U}_{ag}$) winds (Fig. 8). Between 06Z/18 (not shown) and 09Z/18 (Fig. 8a2), $\underset{\sim}{U}_{ag}$ increases dramatically along the South Carolina coast from 9 m s^{-1} (not shown) to a distinct east-southeasterly, 27 m s^{-1} maximum by 09Z/18. This sudden enhancement in the magnitude of $\underset{\sim}{U}_{ag}$ within 3 h is a measure of the increasingly unbalanced flow regime that develops along the coast as the simulated coastal front begins to develop.

The changes in the magnitude of $\underset{\sim}{U}$ lag that for $\underset{\sim}{U}_{ag}$ along the South Carolina coast, increasing from 9 m s^{-1} at 06Z/18 (not shown) to 19 m s^{-1} by 09Z/18 (Fig. 8a1). This lag in the response of $\underset{\sim}{U}$ to the large values of $\underset{\sim}{U}_{ag}$ along the coast persists through the the following 3 h. The southeasterly $\underset{\sim}{U}_{ag}$ along the South Carolina coast increases to 36 m s^{-1} at 10Z/18 (Fig. 8b2), to 39 m s^{-1} by 11Z/18 (Fig. 8c2), and finally stabilizes near 37 m s^{-1} by 12Z/18 (Fig. 8d2). The magnitude of $\underset{\sim}{U}$ continues to increase during the entire 3-h period (Figs. 8a1, 8b1, 8c1, and 8d1), exceeding 30 m s^{-1} over western South Carolina by 12Z/18.

To isolate the processes which contribute to the development of the LLJ, a trajectory is shown for a parcel that passes through the low-level wind maximum in FULL PHYS which is compared to a parcel trajectory computed for ADB (Fig. 9). The trajectories are obtained in the following manner: A parcel near the area of the 850 mb wind maximum in South Carolina at 12Z/18 is selected to initialize the trajectory for FULL PHYS. A backward trajectory is computed for the period between 00Z/18 and 12Z/18 and a forward trajectory for the period between 12Z/18 and 18Z/18 (Fig. 9a). A similar procedure is used to initialize a trajectory for ADB which passes through a wind maximum at 875 mb in South Carolina between 10Z/18 and 12Z/18 (Fig. 9b). Both trajectories are generated in the manner described by Uccellini et al. (1987) using model data every 15 min.

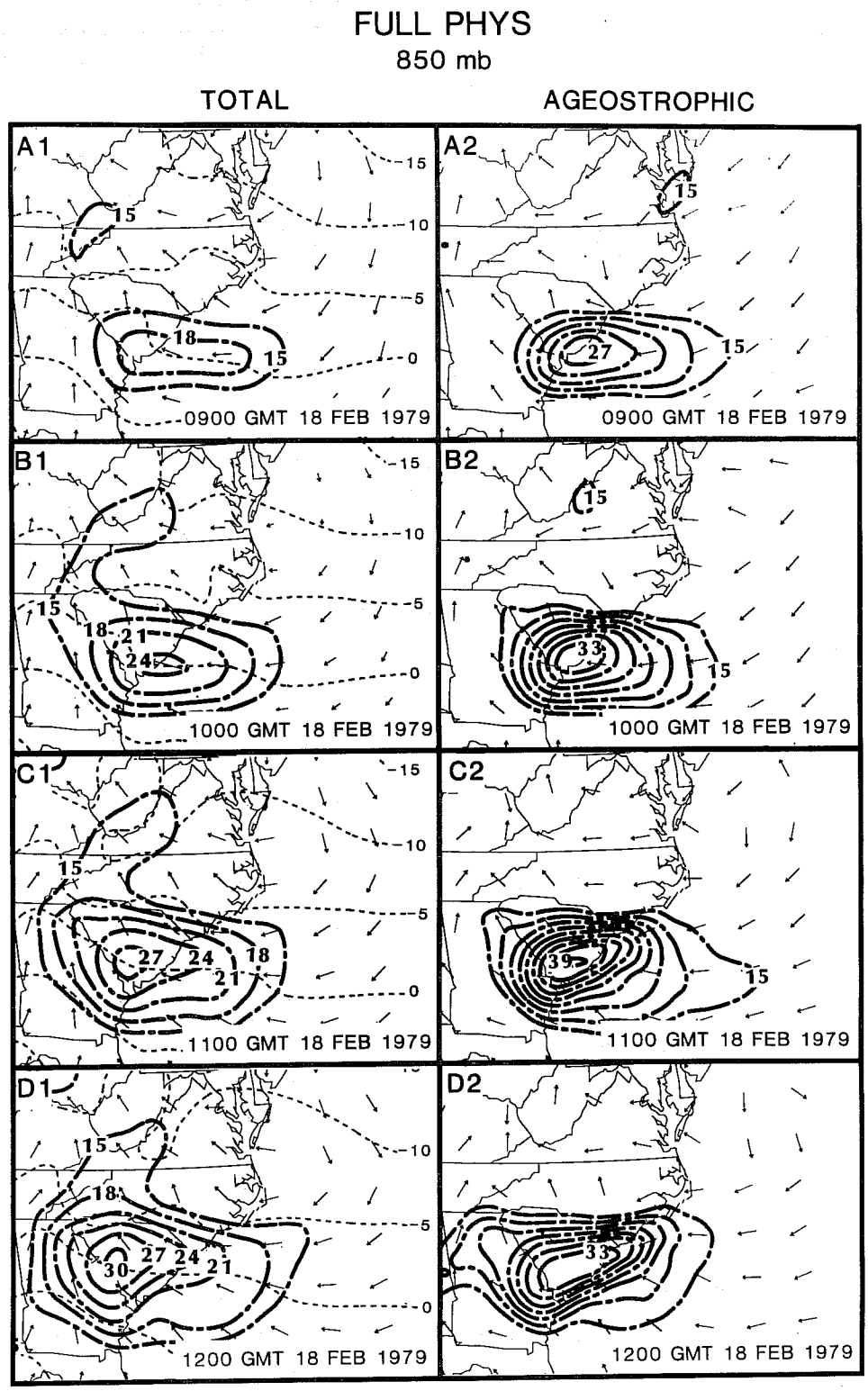

Fig. 8. *Hourly sequence of 850 mb wind direction (arrows) and isotachs (dot-dashed, m* s^{-1}*), total wind (left column; a1, b1, c1, d1) with isotherms included (dashed, °C), and for ageostrophic wind (right column; a2, b2, c2, d2) from the full physics simulation (FULL PHYS).*

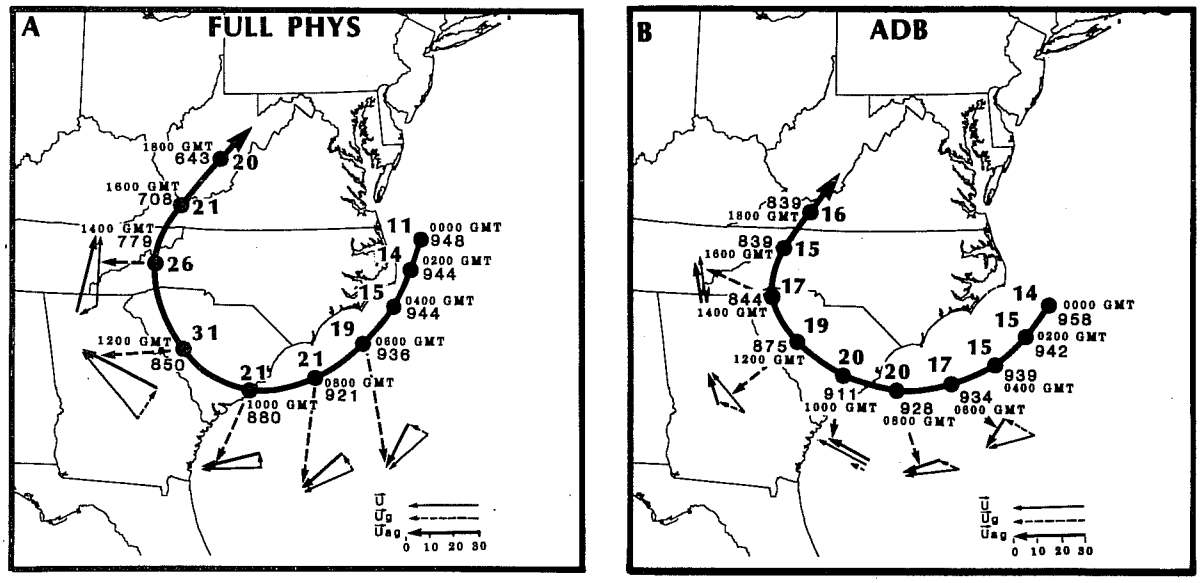

Fig. 9. *Low-level trajectory from the (a) full physics simulation (FULL PHYS) and (b) adiabatic simulation (ADB) initialized as described in Section 5. Two-hourly positions, total wind speed (m s^{-1}), and pressure (mb) indicated. Vector representation for total wind (v), geostrophic wind (v_g), and ageostrophic wind (v_{ag}) presented at 2-h intervals from 0600 through 1400 GMT. Vectors defined and lengths scaled (m s^{-1}) in bottom-right corner.*

To represent the balance of forces affecting the acceleration of parcels, $\underset{\sim}{U}_g$ (the geostrophic wind), $\underset{\sim}{U}_{ag}$, $\underset{\sim}{U}$, and pressure are also displayed in Fig. 9. The $\underset{\sim}{U}_g$ vector can be used as a measure of the pressure gradient force experienced by the parcel at a given time. The $\underset{\sim}{U}_{ag}$ vector is a measure of the imbalance between the pressure gradient and Coriolis forces, with instantaneous accelerations directed to the right of $\underset{\sim}{U}_{ag}$.

The ADB trajectory experiences a relatively weak pressure gradient force as it propagates first toward the southwest before 06Z/18 (Fig. 9b). As the parcel approaches the coast between 06Z/18 and 10Z/18, it accelerates to 20 m s^{-1} and ascends from 934 to 911 mb. This acceleration occurs within the lower branch of the indirect circulation as the parcel maintains a $\underset{\sim}{U}_{ag}$ directed to the left of $\underset{\sim}{U}_g$ (Fig. 9b). The wind speed of 20 m s^{-1} at 10Z/18 represents the maximum attained by the adiabatic trajectory east of the Appalachian Mountains as the $\underset{\sim}{U}$ vector rotates from a direction to the left of $\underset{\sim}{U}_g$ at 08Z/18, consistent with parcel acceleration, into a direction toward the right of the geostrophic vector by 12Z/18, consistent with parcel deceleration (see Fig. 9b). The parcel decelerates after 12Z/18 and turns anticyclonically toward the north and then northeast.

The $\underset{\sim}{U}_g$, $\underset{\sim}{U}_{ag}$, and $\underset{\sim}{U}$ components for the FULL PHYS trajectory (Fig. 9a) differ from its adiabatic counterpart. Between 06Z/18 and 12Z/18, $\underset{\sim}{U}$ for the FULL PHYS parcel is directed at a significantly greater angle to the left of $\underset{\sim}{U}_g$ and for a longer period of time than its adiabatic counterpart as the parcel ascends from 936 to 850 mb. When the parcel ascends from 921 mb at 08Z/18 to 880 mb at 10Z/18, the magnitude of $\underset{\sim}{U}_{ag}$ increases rapidly to 28 m s^{-1} and the angle between $\underset{\sim}{U}$ and $\underset{\sim}{U}_g$ remains large. Given that this imbalance is sustained over a significant portion of the trajectory due to the change in the pressure gradient force, the parcel begins to accelerate at 10Z/18 and turns to the right toward the general direction of the low-level geostrophic wind vector. As the parcel ascent increases from -5.7 to -8.7 μb s^{-1} between 09Z/18 and 10Z/18, it rapidly approaches 850 mb by 12Z/18 during the parcel's interaction with the coastal front. The vertical shear of the geostrophic wind in this area is such that an angle exceeding 80° is maintained between $\underset{\sim}{U}$ and $\underset{\sim}{U}_g$ through 12Z/18, and consequently the magnitude of $\underset{\sim}{U}_{ag}$ continues to increase and exceeds 30 m s^{-1}. Thus, the parcel turns to the right and rapidly accelerates toward the northwest. It is not until after 13Z/18 that $\underset{\sim}{U}$ becomes directed to the right of the $\underset{\sim}{U}_g$ and the parcel begins to decelerate as it continues to rise through the 700 mb level (an ascent that is related, in part, to latent heat release as indicated by the increasing θ and decreasing q in Table 4).

Table 4. Listing for lower-level trajectories from adiabatic simulation (ADB) and full physics simulation (FULL PHYS) (Fig. 9) as described in Section 4. Total wind ($\underset{\sim}{U}$), geostrophic wind ($\underset{\sim}{U}_g$), and ageostrophic wind ($\underset{\sim}{U}_{ag}$) are given in direction and speeds and are in degrees and m s^{-1}, respectively (325 30 = 325°, 30 m s^{-1}), and pressure (p) is in mb. Potential temperature (θ) is in K and mixing ratio (q) is in g kg^{-1}.

HOUR	Low-Level Trajectory from ADB									Low-Level Trajectory from FULL PHYS								
	$\underset{\sim}{U}$		$\underset{\sim}{U}_g$		$\underset{\sim}{U}_{ag}$		θ	p	q	$\underset{\sim}{U}$		$\underset{\sim}{U}_g$		$\underset{\sim}{U}_{ag}$		θ	p	q
04Z/18	63	15	100	7	38	10	277	939	2.3	36	15	83	13	336	12	275	944	3.2
06Z/18	79	17	118	11	39	11	277	934	2.3	50	19	124	6	30	18	278	936	4.0
08Z/18	95	20	113	7	86	13	277	928	2.2	71	21	149	7	51	21	282	921	4.7
09Z/18	105	19	115	6	100	13	277	921	2.1	78	21	183	4	67	22	283	907	4.9
10Z/18	117	20	118	3	116	17	277	911	2.0	94	21	249	8	87	28	284	880	4.6
11Z/18	129	20	132	7	127	13	277	894	1.5	120	27	246	19	97	41	285	857	4.3
12Z/18	138	19	113	7	150	13	277	875	1.7	138	31	218	12	116	32	285	850	4.2
14Z/18	170	17	182	2	169	15	278	844	2.0	181	26	62	6	192	30	289	779	3.5
16Z/18	205	15	219	10	182	6	281	839	2.3	215	21	212	14	216	8	291	708	2.6
18Z/18	228	16	226	5	229	22	281	839	2.3	218	20	220	19	142	1	283	643	1.7

The trajectory from FULL PHYS confirms that the initial acceleration of the parcel and its change in direction from a northeast, to a more east, then a southeast direction is related to the initial modest change in the pressure gradient force experienced by the parcel (as indicated by the change in direction of $\underset{\sim}{U}_g$ listed in Table 4). This change is principally due to the westward movement of the parcel toward the developing coastal trough where the pressure gradient force is changing with time. However, the large imbalance represented by the sudden increase in the magnitude of $\underset{\sim}{U}_{ag}$ to values approaching 40 m s^{-1} at 11Z/18 (Fig. 8c2) is principally due to the vertical displacement of the parcel through the baroclinic region associated with the coastal front.

These trajectory results agree with Durst and Sutcliffe's (1938) and Godson's (1950) hypothesis on the association between organized vertical motion patterns and horizontal acceleration. The results also confirm Newton and Palmén's (1963) discussion (p. 115) of the relationship between vertical motion and parcel acceleration. In effect, the rapid development of the LLJ within 3 h represents a three-dimensional adjustment process in which parcels respond to changing pressure gradient forces due not only to horizontal displacement, but also to their vertical displacement within a baroclinic environment.

5. EFFECTS OF THE LLJ ON SURFACE CYCLOGENESIS AND UPPER-LEVEL FEATURES NEAR THE STJ

The results from the Section 3 show that dynamic and diabatic processes combine to produce the development of an inverted trough along the coast that represents the initial phase of secondary cyclogenesis as the primary surface trough remains west of the Appalachian Mountains. Between 12Z/18 and 00Z/19, the lowest pressure in the inverted trough decreases at a rate of approximately 1 mb h^{-1}. During this initial development phase, the cyclonic circulation appears to be confined to the lower troposphere. As shown by Uccellini et al. (1984, 1985) and Bosart and Lin (1984), a second phase of explosive development commences as a polar jet/trough system approaches the coast around 06Z/19, when the surface cyclone deepens at a rate of 3 mb h^{-1} and the cyclonic circulation extends through a deeper portion of the troposphere.

In FULL PHYS, the concentration of the initial pressure falls along the coast occurs simultaneously with the rapid development of the LLJ. This linkage is consistent with Kocin and Uccellini's (1985a,b) survey of 18 cases of major East Coast snowstorms, for which 1) the LLJ is generally directed from east-southeast toward the west-northwest at a significant angle to the coastline and 2) the SLP appears to decrease as the LLJ develops on the anticyclonic side of an upper-level jet (usually in the exit region of a polar jet).

In this section, the association between the LLJ and the early phase of secondary cyclogenesis is described. A feedback mechanism is also discussed in which the LLJ is related to the enhancement of the cross-contour upper-level ageostrophic flow and associated divergence along the axis of the STJ which contributes further to cyclogenesis and heavy precipitation.

5.1 The relationship of the LLJ to the surface pressure falls along the coast

To determine the effect of the LLJ in the initial decrease of SLP, the mass flux divergence is computed through 21Z/18 (Fig. 10) for the areas indicated in the map inset in Fig. 11. The areas coincide with both the region of maximum SLP falls (as measured by 3-h tendencies) and the entrance region of the LLJ as simulated in FULL PHYS. The mass flux divergence, which is averaged for 44 grid points within the areas, is related to the surface pressure tendency by

$$\frac{\partial p_s}{\partial t} = + \int_{\sigma=1}^{\sigma=0} \nabla_\sigma \cdot \left(\frac{\partial p}{\partial \sigma} \underset{\sim}{U}\right) d\sigma \ , \qquad (1)$$

in which $\partial p/\partial \sigma$ is a measure of mass between sigma surfaces.

At 06Z/18, the mass divergence profile for FULL PHYS indicates relatively weak mass divergence in three layers over the Southeast Coast, one centered near 650 mb, another near 400 mb, and one near 200 mb (Fig. 10a1). This profile is representative of the mass divergence structure at the end of the first 6 h in which the model simulated a decrease of SLP only 2 mb. While a deeper layer of mass divergence develops between 700 and 300 mb by 12Z/18, the mass divergence in the layer below 800 mb increases by an order of magnitude to near 20×10^{-3} mb s^{-1} (Fig. 10a1). This increase in the

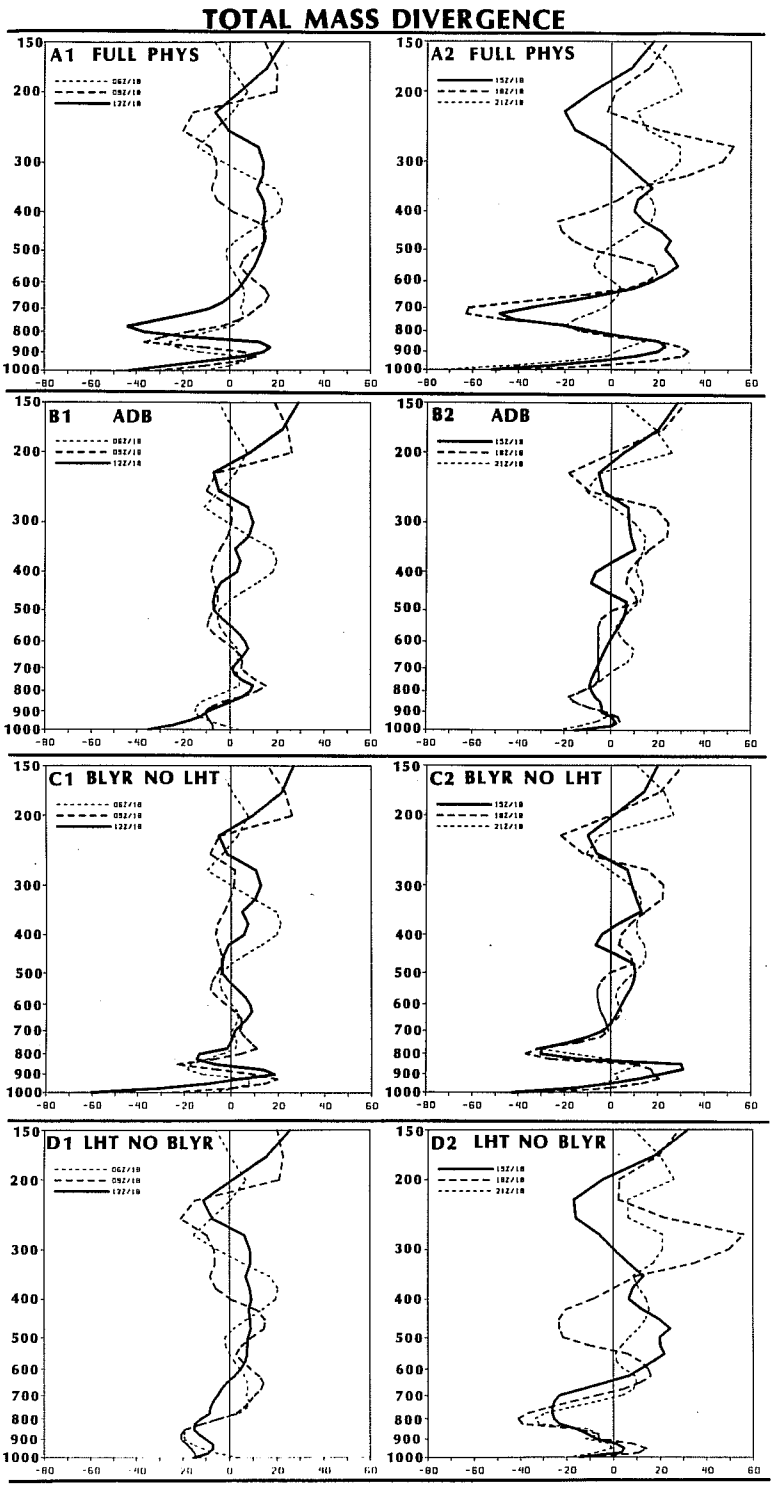

Fig. 10. *Vertical profiles of area-averaged mass flux divergence ($10 = 10 \times 10^{-3}$ mb s^{-1}) computed for 0600 GMT (thin dashed), 0900 GMT (thick dashed), and 1200 GMT (solid) in the left column and 1500 GMT (solid), 1800 GMT (thick dashed), and 2100 GMT (thin dashed) in the right column: (a) profiles from full physics simulation (FULL PHYS); (b) profiles from adiabatic simulation (ADB); (c) profiles from boundary layer simulation with no latent heat (BLYR NO LHT); (d) profiles from latent heat simulation with no boundary layer (LHT NO BLYR). The profiles are computed from the areas along the Georgia to Middle-Atlantic coasts depicted on map inset for times shown in Fig. 11.*

low-level mass divergence coincides with the rapid development of southeasterly winds in the western portion of the volume without a similar increase in the eastern portion (i.e., the entrance region of the LLJ) and contributes, in part, to a 4 to 5 mb decrease in the SLP along the Carolina coast between 06Z/18 and 12Z/18 [see Fig. 15 in Uccellini et al. (1987)]. Also evident from 09Z/18 through 15Z/18 is a shallow layer of mass convergence below the 900 mb level, which is consistent with the increasing absolute vorticity associated with the developing inverted trough along the coast. By 18Z/18, the relative maximum in the mass divergence still persists near 900 mb within the entrance region of the LLJ, increasing to 32×10^{-3} mb s^{-1} (Fig. 10a2). Simultaneously, the upper-level divergence also increases in magnitude. Between 18Z/18 and 21Z/18, the low-level mass divergence begins to diminish and a more organized upper-level divergence pattern becomes the dominant factor, as the STJ and its associated divergence pattern shift southward.

The mass divergence profiles computed for ADB (Figs. 10b1 and 10b2), BLYR NO LHT (Figs. 10c1 and 10c2), and LHT NO BLYR (Figs. 10d1 and 10d2) illustrate the contribution of the various physical processes to the initial development of this storm. The mass divergence profiles for ADB display only a weak maximum near 800 mb at 09Z/18 and 12Z/18 and a more organized upper-level maximum after 18Z/18. The low-level maximum develops as southeasterly winds in the lower branch of the indirect circulation increase with time. However, since the magnitudes of the maximum wind speed and associated horizontal gradients are weaker for the LLJ in ADB (note that the increase of wind speed along the low-level trajectory in Fig. 9b is only 2 m s^{-1} between 06Z/18 and 12Z/18), the lower-tropospheric mass divergence remains smaller than in FULL PHYS. The magnitude of the upper-level divergence also remains smaller in ADB throughout the entire 24-h simulation.

In BLYR NO LHT, the mass divergence profiles (Figs. 10c1 and 10c2) are dominated by a pronounced maximum in the mass divergence near the 850 mb level that develops between 06Z/18, 09Z/18, and 12Z/18, during which time the SLP begins to decrease and an inverted trough develops. The striking feature in this simulation is that above 700 mb, the mass divergence profiles for BLYR NO LHT are very similar to the ADB profiles, indicating that the initial development of the inverted trough prior to 15Z/18 in BLYR NO LHT is primarily related to the low-level divergence maximum. However, the lack of deepening of the inverted trough <u>after</u> 15Z/18 is probably related to the minimal development of the upper-level divergence (Fig. 10c2) when compared to that in FULL PHYS (Fig. 10a2).

For the LHT NO BLYR simulation, the mass divergence profiles illustrate that the impact of the latent heat release is generally maximized above 700 mb, where the divergence profiles (Figs. 10d1 and 10d2) are nearly identical to those from FULL PHYS. However, below 700 mb, the LHT NO BLYR profiles are similar to those from ADB with no indication of a sustained low-level mass divergence maximum when latent heat is the only physical process included in the model simulation. Given that the major difference between the FULL PHYS and LHT NO BLYR divergence profiles is confined to the lower troposphere, it appears that the lack of mass divergence near 850 mb could account for the lack of development of an inverted trough along the Southeast coast in this simulation (Fig. 7).

These results demonstrate that 1) the PBL physics and latent heat release have a significant effect on the lower- and upper-level mass divergence maxima, respectively, 2) the initiation of the secondary cyclogenesis along the coast is strongly influenced by the low-level mass divergence in the entrance region of a rapidly developing LLJ which acts to focus SLP falls along the coast, and 3) the continued development of the inverted trough and cyclone along the coast prior to 00Z/19 is sustained by the upper-level mass divergence along the axis of the STJ that is enhanced by the latent heat release.

5.2 Effect of LLJ development on the upper-level features

As shown by Uccellini et al. (1984), the decreasing distance between an upper-level trough approaching the East Coast and a ridge downstream of the trough axis contributes to parcel accelerations and associated increasing upper-level divergence along the axis of the STJ near the ridge crest at 12Z/18. The decreasing wavelength is due to the decrease in the propagation rate of the ridge without a corresponding decrease in the eastward propagation rate of the trough in the central United States. Using a quasi-geostrophic approach, Atlas (1987) shows that the decreasing wavelength during the period of rapid cyclogenesis on 19 February increases the vorticity gradient between the trough and ridge axes and thereby contributes to an increase of vorticity advection and associated upper-level divergence over the cyclone during its rapid development phase.

As indicated in the map inset in Fig. 11, the 332 K ψ values are larger near the ridge axis in FULL PHYS when compared to ADB. The increases in ψ are associated with a more pronounced ridge and slower eastward displacement of the 332 K ridge crest in FULL PHYS, which is also reflected by the 3-h ψ tendency field over the Appalachian region where the ψ falls

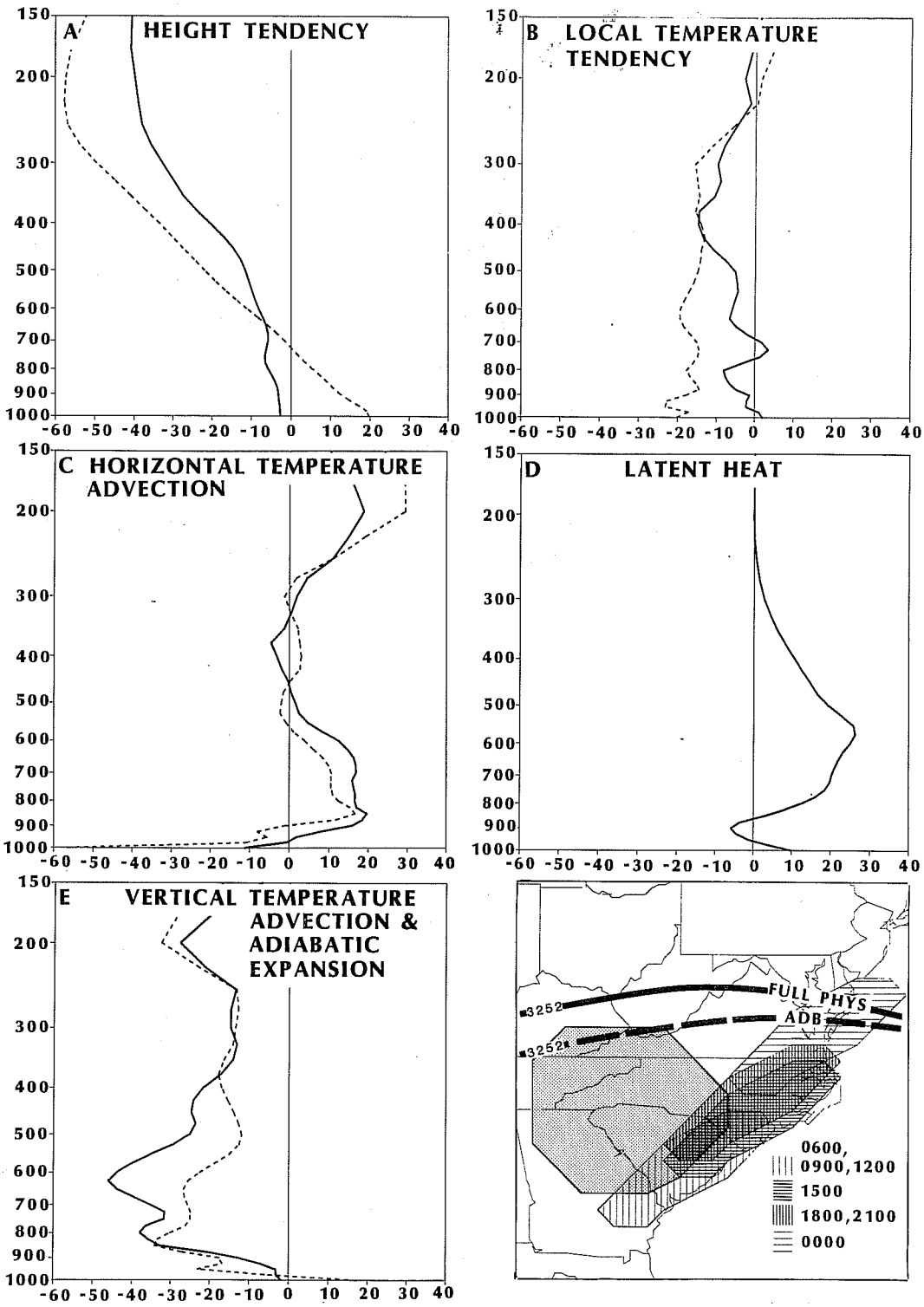

Fig. 11. *Vertical profiles of area- and time-averaged tendencies for a 3-h period between 0900 and 1200 GMT 18 February 1979 for the lightly shaded inland region in the map inset: (a) geopotential height (20 = 20 m height change over 3 h); (b) local temperature (K day^{-1}) changes; (c) temperature changes (K day^{-1}) due to horizontal temperature advection; (d) temperature changes (K day^{-1}) due to latent heat release; (e) vertical temperature advection and expansion. Solid lines are for the full physics simulation (FULL PHYS) and dashed lines are for the adiabatic simulation (ADB), where applicable. The position of a representative ψ_m contour (3.252 x 10^5 m^2 s^{-2}) is also shown in map inset for ADB (dashed) and FULL PHYS at 1200 GMT 18 February (solid).*

in ADB are twice as large as in FULL PHYS (not shown). For the area depicted in the map inset (Fig. 11), the difference between the adiabatic and full physics simulations is reflected by the profiles of the geopotential height (ϕ) tendency derived on pressure surfaces between 09Z/18 and 12Z/18 (Fig. 11a). The vertical profiles of the ϕ tendency are significantly less negative above 700 mb for FULL PHYS due principally to the large differences in the local temperature tendencies for the same region (Fig. 11b). In ADB, 15 to 20 K day^{-1} cooling rates are diagnosed between 950 and 500 mb, while FULL PHYS cooling rates generally range between 0 and 10 K day^{-1} below 500 mb, resulting in smaller negative ϕ tendencies and thus a slower eastward displacement of the ridge.

To assess the relative importance of the various physical processes that could act to reduce the cooling rates and enhance the magnitude of the upper-tropospheric ridge, the thermodynamic equation is calculated as follows:

$$\frac{\partial T}{\partial t} = \underset{\sim}{U}\cdot\nabla_p T + \frac{Q}{c_p} - \omega\left(\frac{\partial T}{\partial p} - \frac{RT}{c_p p}\right) \qquad (2)$$

(where Q is the heating rate due to latent heat release, c_p is specific heat under constant pressure, and R is the universal gas constant). All the terms on the right-hand side of eq. (2) are averaged over the 3 h between 09Z/18 and 12Z/18 for the area shaded in the map inset in Fig. 11 for ADB and FULL PHYS.

A significant difference exists between these two simulations for all three terms in eq. (2). Warm air advection is larger in FULL PHYS throughout the entire troposphere below 450 mb, with the maximum advection located near 850 mb (Fig. 11c). The increased warm air advection associated with the general increase in the magnitude of the low-level winds in FULL PHYS accounts for a significant portion of the difference in the local temperature tendency beneath the 800 mb level. Heating rates of 10 to 25 K day^{-1} associated with latent heat release between 800 and 450 mb (Fig. 11d) are slightly larger than the maximum warming associated with the warm air advection below 700 mb and contribute significantly to the difference in the local temperature tendency between ADB and FULL PHYS, especially above 750 mb. The last term in eq. (2), which combines the effects of vertical temperature advection and adiabatic expansion and acts to offset the warming effects of the other two terms, is negative throughout for both

simulations. The increased horizontal temperature advection associated with the development of the LLJ combined with latent heat release is sufficient to offset the greater cooling associated with the enhanced ascent pattern in FULL PHYS to produce a relatively warmer domain and better-defined upper-level ridge compared to ADB.

6. SUMMARY

A series of numerical simulations of the Presidents' Day cyclone isolates the active roles of upper-tropospheric jet streaks, the oceanic PBL, and latent heat release in the secondary cyclogenesis observed along the East Coast of the United States on 18-19 February 1979. Model simulations with and without diabatic processes associated with heat and moisture fluxes in the oceanic PBL and grid-resolvable and convective precipitation show that these processes, in conjunction with the jet streak circulation patterns, are necessary for the initial development of the storm system along the coast. However, neither the jet alone nor the combinations of either the jet-induced circulation with latent heat release or the jet-induced circulation with PBL processes is sufficient to yield a satisfactory simulation of the LLJ and the initial phase of secondary cyclogenesis. Therefore, a synergistic interaction must exist among these processes to account for the secondary cyclogenesis and associated rapid changes in the mass, momentum, and moisture fields for this case.

The numerical simulations indicate the following sequence of events marked the initial development phase of the Presidents' Day cyclone:

1) Increasing divergence along the axis of an upper-tropospheric STJ is associated with the development of an indirect circulation displaced to the anticyclonic side of the STJ that extends through the entire depth of the troposphere. The lower branch of the indirect circulation amplifies over the southeastern United States with a significant ageostrophic wind component directed from the oceanic PBL across the coastline toward the Appalachian Mountains.

2) Sensible heating and moisture flux within the oceanic PBL reduce the static stability east of the Carolina coast. Furthermore, the heat and moisture fluxes warm and moisten the lower branch of the indirect circulation, enhancing precipitation rates and latent heat release west of the coastline.

3) The sloped orientation of the lower-tropospheric isentropic surfaces west of the coastline, the merging of the lower branch of the indirect circulation associated with the STJ and the upper branch of a direct circulation associated with the coastal front and latent heat release all

contribute to a significant vertical displacement of parcels crossing the coastline within the lower branch of the indirect circulation.

4) The vertical displacement of the parcels in a baroclinic environment (in which both the magnitude and direction of the pressure gradient force change significantly with height) is associated with a rapid increase in the magnitude of the ageostrophic wind component along the coast within a 2- to 3-h period. This imbalance subsequently leads to parcel acceleration and to the rapid formation of a LLJ that slopes upward from the oceanic PBL toward the 700 mb level over the Appalachian Mountains.

5) The accelerations associated with the developing LLJ are responsible for a sudden increase in the lower-tropospheric mass flux divergence in the entrance region of the LLJ. The mass divergence maximum in the entrance region of the LLJ is an important factor in focusing the decrease in SLP along the Southeast Coast that constitutes the initial development phase of the secondary cyclone as the primary surface system weakens and fills over the Ohio Valley.

6) The development of the LLJ enhances the warm air advection and moisture flux to the north and west of the developing surface low. The increased warm air advection and latent heat release (associated with resolvable grid-scale precipitation) act to increse the magnitude of the upper-level ridge. Furthermore, the propagation rate of the upper-level ridge is decreased while the upper-level trough over the central United States continues to propagate eastward, effectively reducing the wavelength between the trough and ridge axes.

The processes involved in the development of the LLJ, coastal cyclogenesis, and the enhancement of the upper-level ridge interact in a mutually supportive way. The sensible and latent heating in the ocean-influenced PBL and coastal frontogenesis contribute to the vertical displacement of parcels entering the LLJ, resulting in significant ageostrophy and subsequent horizontal accelerations. These accelerations contribute to the decrease of the SLP along the coast and to the increase in 1) the magnitude of the warm air advection, 2) moisture transport over a broad region in the southeastern United States, and 3) the precipitation and associated latent heat release. The warm air advection and latent heat release act to enhance the magnitude of the upper-level ridge and slow its eastward movement as the trough approaches the East Coast from the central United States. Parcels moving along the axis of the STJ approach the ridge axis, cross toward lower ψ_m values, and accelerate. The acceleration, associated with the decreasing distance between the trough and ridge axes, is accompanied by increasing upper-level divergence. The upper-level divergence enhances the ascending branch of the indirect circulation in

which the LLJ is embedded. The process thereby supports further development of the LLJ and surface cyclone.

This sequence represents a positive feedback mechanism which sustains the early development of the Presidents' Day cyclone in a manner which is similar to the "self-development" concept identified by Sutcliffe and Forsdyke (1950) and discussed by Palmén and Newton (1969, pp. 324-326). If the low-level warming related to temperature advections or diabatic processes is not sufficiently strong, the upper-level divergence between the trough and the ridge axes will not increase, thus disrupting the feedback effect that perpetuates the development of the LLJ and associated temperature advection and low-level mass divergence patterns that are focused along the Southeast Coast. This disruption occurs after 15Z/18 in ADB, BLYR NO LHT, and LHT NO BLYR. These three simulations lack the sustained warming associated with temperature advection and diabatic processes which contribute to the mass divergence maxima in the lower and upper troposphere needed to support the continued development of the surface trough for this case.

This model experiment indicates that, since the dynamic and diabatic processes act in a synergistic manner, it is not possible to designate one process as more important than another for the formation of this coastal storm. Furthermore, it is difficult to separate the relative importance of upper- and lower-tropospheric forcing mechanisms since processes near the top and bottom of the troposphere interact to influence the evolution of the jet streak system, surface cyclone, and associated vertical circulation patterns diagnosed throughout the entire extent of the troposphere.

7. ACKNOWLEDGMENTS

The authors thank Miss Kelly Wilson for typing the manuscript. Discussions with Drs. Michael Kaplan, Daniel Keyser, John Zack, and Lance Bosart have been helpful during the course of this study. Thanks to Mr. Robert Aune (STX Systems Corporation) and Mr. Jeffrey Whitaker (Florida State University) for their help in developing model and post-processing software used in this study.

8. REFERENCES

References for this paper are listed at the end of part II.